Nonlinear Dyn (2018) 91:609–624
https://doi.org/10.1007/s11071-017-3897-z

ORIGINAL PAPER

Dynamic response of masonry arch with geometrical irregularities subjected to a pulse-type ground motion

L. Severini · N. Cavalagli · M. DeJong · V. Gusella

Received: 11 May 2017 / Accepted: 22 October 2017 / Published online: 3 November 2017

Abstract Ancient masonry structures often rely on the masonry arch as a load bearing element. The understanding of its response under seismic actions is a first fundamental step towards the comprehension of the behaviour of more complex structures. It is well known that the stability of masonry arches is primarily related to the geometry. The safety assessment under seismic actions is usually carried out by considering known deterministic geometrical parameters, such as thickness, rise and span, and the voussoirs are assumed with equal dimensions. However, many factors, like defects or irregularities in the shape of the voussoirs and imprecise construction, produce variations of the geometry with respect to the nominal one and, as a consequence, may effect the ability of the arch to resist seismic actions. In this paper, the effect of geometrical irregularities on the dynamic response of circular masonry arches is considered. Irregular geometries are obtained through a random generation of the key geometrical parameters, and the effect of these irregularities is quantified by analysing the dynamic response to ground motion. The masonry arch is modelled as a four-link mechanism, i.e. a system made of three rigid blocks hinged at their ends. The position of the hinges at the instant of activation of the motion is determined through limit analysis. Lagrange's equations of motion have been written for the generated irregular geometries and solved through numerical integration. The results are summarised by a fragility surface that quantify the extent to which geometrical uncertainties can alter the dynamic response of the masonry arch and increase its seismic vulnerability.

Keywords Masonry arch · Geometrical irregularities · Dynamic analysis · Limit analysis

L. Severini (✉)· N. Cavalagli · V. Gusella
Department of Civil and Environmental Engineering, University of Perugia, Via G. Duranti 93, 06125 Perugia, Italy
e-mail: laura.severini@strutture.unipg.it

N. Cavalagli
e-mail: nicola.cavalagli@unipg.it

V. Gusella
e-mail: vittorio.gusella@unipg.it

M. DeJong
Department of Engineering, University of Cambridge, Trumpington Street, Cambridge CB2 1P, UK
e-mail: mjd97@eng.cam.ac.uk

1 Introduction

Masonry constructions represent a significant portion of the world's heritage building stock. Seismic events have produced severe damages to these structures, highlighting the need to better understand their behaviour to protect the human life and cultural heritage. Arch-type elements are common in masonry constructions. The knowledge of their seismic response is a fundamental objective to understand how seismic loads can be transmitted though the masonry bearing elements of complex structures and to define an adequate

reinforcement [2]. In this context, masonry constructions often show the presence of geometrical irregularities associated with imprecise construction or structural degradation due to environmental actions. Hence, the understanding of the influence of these geometrical irregularities on collapse is necessary for adequate safety assessment.

The static analysis of arches and vaults is often carried out using limit analysis, based on the well-known assumptions [14,15]: (i) masonry has no tensile strength, (ii) the compressive strength of masonry is infinite and (iii) sliding does not occur. This approach represents an effective tool for a rapid safety assessment of masonry constructions and is based on the assumption that the equilibrium condition, the yield criterion and the mechanism condition must be satisfied at collapse. In other terms, collapse occurs for the maximum load at which a thrust line, in equilibrium with the acting loads and passing through all joints of the masonry arch, can be found. The evaluation of the load multiplier that activates the kinematic chain is essentially a stability problem, not related to the strength of the material. Hence, the collapse behaviour is assumed to be governed by the shape and geometry of the arch, rather than by material properties [13]. In this framework, the effect of the earthquakes can be approximated by static-equivalent horizontal forces [11].

The problem of the influence of uncertainties on the stability of masonry structures has been addressed by some authors, following different approaches. Psycharis et al. [19] investigated the loss of stability due to imperfections, with reference to the classical problem of free-standing columns, by means of the distinct element method, taking into account the uncertainty related to the initial tilt of the column or the reduction of contact area due to edge damage. The effect of geometrical uncertainties on the bearing capacity of masonry arches has been studied by some authors in the framework of the equilibrium analysis of rigid body mechanism [1,3,20,21] or by means of the finite elements method [22], considering the irregularity of the structure through the regeneration of real geometry, the identification of a local defect or modelling the uncertainty related to the shape of each constitutive stone element of the arch. A different approach has been proposed in [4] where the limit analysis is carried out taking into account the geometrical uncertainties modelled as random variables.

It should be noted that limit analysis can provide the horizontal load multiplier that turns the structure into a mechanism, but the evolution of the dynamic motion cannot be analysed. Moreover, to the knowledge of the authors, there are no contributions dealing with the influence of geometrical uncertainties on the dynamic behaviour of the masonry arch.

The single rocking block provides a simple model that behaves, in essence, similarly to the dynamic response of the masonry arch. Housner [16] studied the overturning of a rigid block subjected to horizontal forces. A dynamic analysis of the circular masonry arch was carried out by Oppenheim, considering an equivalent SDOF system made of three rigid links hinged at their ends [18]. Clemente [5], also investigated free vibrations of the arch, and its response to harmonic base acceleration. DeJong and Ochsendorf [11] investigated the dynamic response with discrete element modelling, and showed that assuming failure due to direct overturning, without rocking, is unsafe. Oppenheim's analytical model was enriched by De Lorenzis et al. [6], taking into account the dissipation of energy caused by the impact. This improved model allows simulation of the motion of the arch through continued cycles of rocking. The analytical predictions were subsequently compared to results from experimental tests on model arches [9]. Recently, using a similar approach, analytical modelling has also been carried out to study the dynamic behaviour of the pointed arch [17]. In addition, a methodology to derive an equivalence between SDOF rocking structures (or mechanisms, e.g. the circular masonry arch) and the single rocking block has been developed by DeJong and Dimitrakopoulos [10]. An interesting investigation on failure domains and collapse modes of masonry arch on buttresses has been carried out in [12], where a parametric study based on the discrete element method has been performed to evaluate the dynamic behaviour and the sensitivity of the response to changes in the excitation, geometry and mechanical parameters.

In this paper, the dynamic response of the masonry arch has been analysed using an analytical model consisting of a four-link mechanism, while taking into account geometrical irregularities described by means of random variables. In the first part, irregular arch geometries are defined and the analytical model adopted for the study of the dynamic response is described. In the second part, dynamic analysis has been performed on the arch geometry considered by

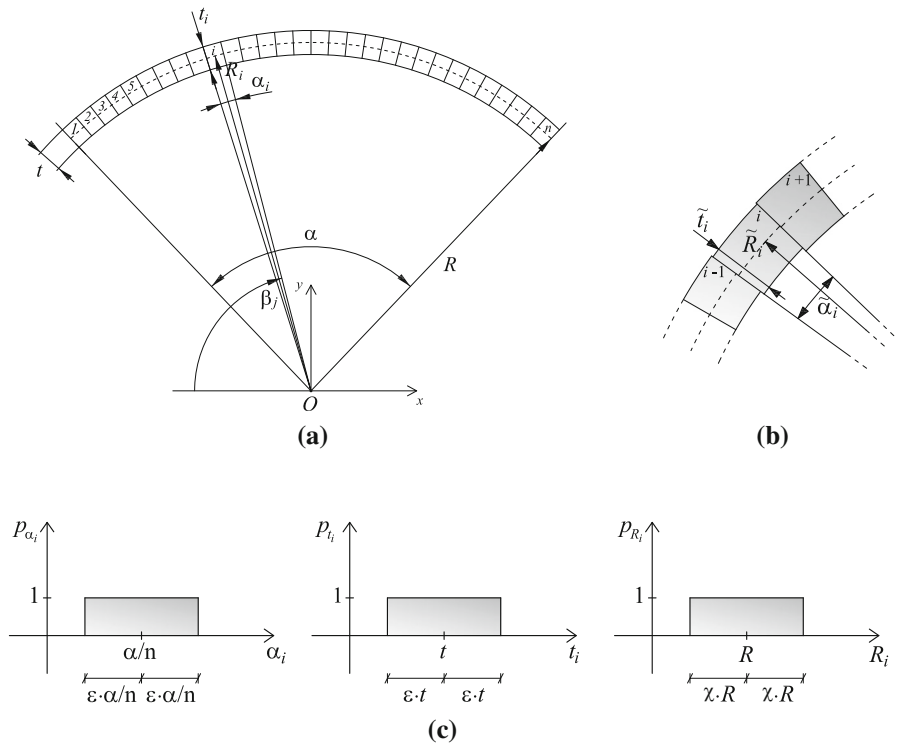

Fig. 1 Geometrical parameters for the definition of the nominal arch shape (**a**), generic uncertain voussoir shape (**b**) and probability density functions of the angle of embrace α_i, the thickness t_i and the radius R_i (**c**) [4]

Oppenheim [18], taking into account the geometrical uncertainties related to imprecise construction, shape defects or deterioration. The response of Oppenheim's arch to step impulse base acceleration has been compared to those of two uncertain geometries, generated from the nominal one. The effects of geometrical uncertainties on dynamic collapse are shown by means of fragility curves.

2 Geometrical model

The deterministic geometry (or *nominal geometry*) of the circular masonry arch has been defined by assigning the radius R, the angle of embrace α and the thickness t. The arch has been discretised into n voussoirs by radial lines passing though the centre O (Fig. 1a).

The uncertain geometry of the masonry arch has been generated by assuming: (i) radial joints, (ii) deterministic value of the angle of embrace α of the whole arch and (iii) uniform probability density functions for the random geometrical parameters (independent variables). The parameters that define the nominal geometry of the arch have been related to each voussoir: α_i, t_i and R_i denote, respectively, the angle of embrace of the generic i-th voussoir, the thickness and radius of the mean circular construction line of the same voussoir. The uncertainties related to the shape of the voussoirs have been modelled by considering these parameters as random variables (Fig. 1b), with uniform probability density functions (Fig. 1c) [4]:

$$\begin{cases} \tilde{\alpha}_i = E[\tilde{\alpha}_i] + \varepsilon\ \alpha/n\ \cdot\ \tilde{p}_{\alpha_i} = \alpha/n + \varepsilon\ \alpha/n\ \cdot\ \tilde{p}_{\alpha_i} \\ \quad = \alpha/n\,(1 + \varepsilon\ \tilde{p}_{\alpha_i}) \\ \tilde{t}_i = E[\tilde{t}_i] + \varepsilon\ t\ \cdot\ \tilde{p}_{t_i} = t + \varepsilon\ t\ \cdot\ \tilde{p}_{t_i} = t\,(1 + \varepsilon\ \tilde{p}_{t_i}) \\ \tilde{R}_i = E[\tilde{R}_i] + \chi\ R\cdot\ \tilde{p}_{R_i} = R + \chi\ R\cdot\ \tilde{p}_{R_i} = R\,(1 + \chi\ \tilde{p}_{R_i}) \end{cases} \tag{1}$$

where ε defines the amplitude of the range of variability, $\chi = \varepsilon\ t/R$ and $\tilde{p}_{\alpha_i}$, $\tilde{p}_{t_i}$, $\tilde{p}_{R_i}$ are random independent samples taken from a uniform probability density function defined in the range $[-1, 1]$. The mean values of the random geometrical parameters have been assumed equal to the corresponding nominal values.

In this paper, the arch geometry analysed by Oppenheim [18] has been considered, with a radius $R = 10$ m, an angle of embrace $\alpha = 157.5°$, a thickness $t = 1.5$ m and a number of voussoirs $n = 7$. This nominal geometry will be hereinafter denoted as "Oppenheim's arch", while in the presence of geometrical uncertainties it

will be called "random Oppenheim's arch". In order to study the behaviour of the masonry arch with geometrical uncertainties in the dynamic field, a value of the tolerance $\varepsilon = 0.10$ has been assumed, corresponding to $\chi = 0.015$. Considering that a value of $\varepsilon = 0.03$ refers to the tolerance prescribed by the standard codes of the industrial production of brick masonry, a tolerance $\varepsilon = 0.10$ appears justifiable when dealing with masonry arches made of natural stones or whose geometry has been modified by environmental factors or imprecise construction. In the following, the dynamic responses of two samples of random Oppenheim's arch, denoted as arch RA-1 and RA-2, have been compared to the nominal one, denoted as NA.

3 Loading system and activation conditions of the mechanism

The arch has been subjected to a horizontal base acceleration $\ddot{x}_g$, as a function of time t. The evaluation of the mechanism activation conditions under the horizontal ground motion has been carried out through limit analysis. Following this approach, each voussoir of the arch has been subjected to a vertical force $F_i = m_i\, g$ and to a horizontal force $F_{S_i} = k\, F_i$, where m_i is the mass of the voussoir and g the gravity acceleration. In order to evaluate the horizontal load multiplier k, the fulfilment of the equilibrium condition, the yield criterion and the mechanism condition has been imposed at collapse. A thrust line in equilibrium with the acting loads, lying inside the boundaries of the arch and corresponding to a four-hinge mechanism has been found [3]. Following this approach, the activation of motion corresponds to a value $\ddot{x}_g/g$ of the horizontal base acceleration greater than or equal to the horizontal load multiplier k. In Fig. 2, the activation conditions of Oppenheim's arch NA, in terms of collapse hinges and thrust line at collapse, are represented. For the nominal geometry, a unique horizontal load multiplier k can be calculated, corresponding to a collapse mechanism denoted by Mech-n; k was found equal to 0.37.

When a random geometry is considered, the load multiplier becomes a random variable $\tilde{k}$; moreover two values of the horizontal load multiplier can be determined for each sample (generated arch), denoted by $\tilde{k}_l$ and $\tilde{k}_r$, because the structure is non-symmetric with respect to the vertical axis passing through the crown.

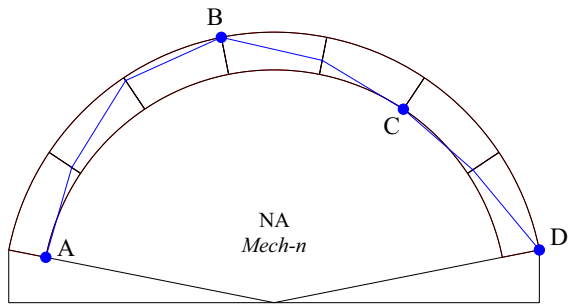

Fig. 2 Collapse hinges and thrust line of Oppenheim's arch NA

These two values of the horizontal load multiplier correspond to different mechanisms, which can be denoted by Mech-l (Fig. 3a) and Mech-r (Fig. 3b), respectively. Hence, the activation of motion could occur at $\tilde{k}_l$ or $\tilde{k}_r$, depending on the relative direction of the ground motion:

$$\begin{cases} \ddot{x}_g(t_0)/g <= -|\tilde{k}_l| & \text{motion starts with Mech-l} \\ \ddot{x}_g(t_0)/g >= |\tilde{k}_r| & \text{motion starts with Mech-r} \end{cases} \tag{2}$$

where t_0 is the initial time and the ground acceleration $\ddot{x}_g$ has a positive sign if directed from left to right. In order to evaluate the activation mechanism of motion, the limit analysis was applied considering horizontal forces acting from left to right. Therefore, in the following, mechanism Mech-r (Fig. 3b) is analysed considering an arch geometry mirrored respect to the vertical direction.

The activation conditions for random Oppenheim's arches RA-1 and RA-2 are shown in Fig. 4. In the same figure, in order to better understand the generated geometry variation, random arches (black colour) are superimposed to Oppenheim's arch NA (red colour). The collapse hinges and the thrust line related to mechanism Mech-l are represented, respectively, in Fig. 4a, c for arch RA-1 and RA-2, while in Fig. 4b, d) mechanisms Mech-r are depicted mirrored respect to the vertical direction. The corresponding horizontal load multipliers for random arch RA-1 are equal to $\tilde{k}_l = 0.4111$ and $\tilde{k}_r = 0.3104$, while for random arch RA-2 it results $\tilde{k}_l = 0.3946$ and $\tilde{k}_r = 0.3501$.

The results of the limit analysis procedure, both in terms of horizontal load multipliers and progressive angle β_j corresponding to the collapse hinges (Fig. 1a), are summarised in Table 1 (for Oppenheim's arch no

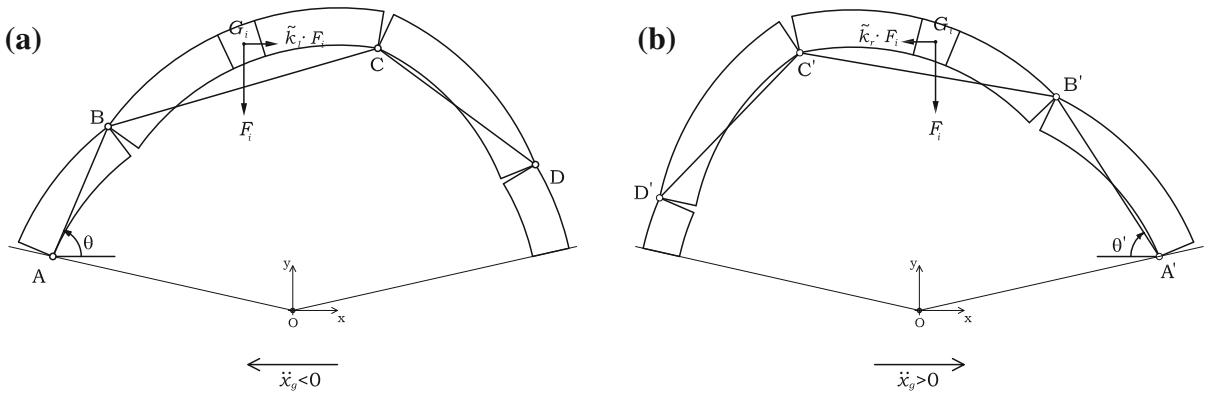

Fig. 3 Mechanism Mech-l (**a**) and Mech-r (**b**) with the corresponding forces acting on the *i*-th voussoir

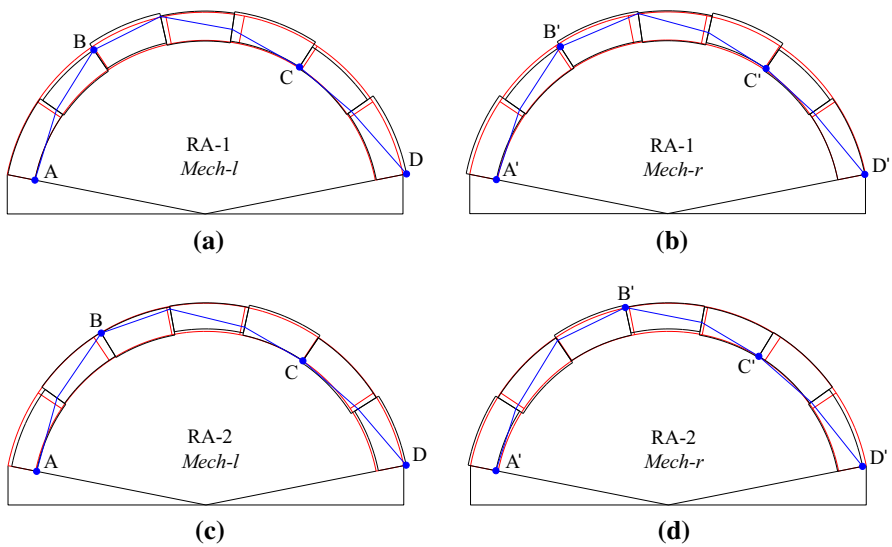

Fig. 4 Collapse hinges and thrust line of random arches RA-1 and RA-2 (black), superimposed to Oppenheim's arch NA (red). Case: **a** mechanism Mech-l for random arch RA-1, **b** mechanism Mech-r mirrored respect to the vertical direction for random arch RA-1, **c** mechanism Mech-l for random arch RA-2, **d** mechanism Mech-r mirrored respect to the vertical direction for random arch RA-2

distinction has been made between Mech-l and Mech-r because a unique collapse mechanism Mech-n can be detected).

4 Analytical model for the dynamic analysis

4.1 Lagrangian coordinate

The dynamic behaviour of the arch has been studied by modelling the structure as a four-link mechanism, following the approach proposed by Oppenheim [18] and with the impact model proposed by De Lorenzis et al. [6]. An equivalent SDOF system made of three rigid blocks has been considered, whose generic displaced configuration can be defined by a unique Lagrangian coordinate. It will be denoted by θ or θ' when referring, respectively, to mechanism Mech-l (Fig. 3a) or Mech-r (Fig. 3b). The value of the Lagrangian coordinate corresponding to the instant of activation of motion, namely to the undisplaced configuration, will be denoted by θ_u (or θ'_u). Hence, each displaced configuration of the arch corresponds to a value $\theta < \theta_u$ (or $\theta' < \theta'_u$).

4.2 Critical rotation angle

Once the mechanism of the arch has been activated, a condition of unstable equilibrium can be identified. This state corresponds to a non-recovery rotation,

Table 1 Activation conditions for the analysed arches in terms of horizontal load multiplier and progressive angle of the collapse hinges

	k	$\tilde{k}_l$	$\tilde{k}_r$	$\beta_{A\,(A')}$ (rad)	$\beta_{B\,(B')}$ (rad)	$\beta_{C\,(C')}$ (rad)	$\beta_{D\,(D')}$ (rad)
NA, Mech-n	0.3700	–	–	0.1963	1.3744	2.1598	2.9452
RA-1, Mech-l	–	0.3946	–	0.1963	0.9749	2.1417	2.9452
RA-1, Mech-r	–	–	0.3501	0.1963	0.9999	2.1667	2.9452
RA-2, Mech-l	–	0.4111	–	0.1963	1.0240	2.1633	2.9452
RA-2, Mech-r	–	–	0.3104	0.1963	1.3562	2.1176	2.9452

namely to a critical value θ_{cr} (or θ'_{cr}) of the Lagrangian coordinate. If the arch is released with zero initial velocity, in the absence of external loads or ground acceleration, in a displaced configuration corresponding to $\theta_0 > \theta_{cr}$ (with $\theta_0 < \theta_u$), it will return to the undisplaced configuration corresponding to θ_u, while for $\theta_0 < \theta_{cr}$ the arch will collapse. With reference to the notation of Fig. 5, e.g. dealing with Mech-l, let us define the law of the potential energy for the equivalent SDOF system [18]:

$$V = g\Big[m_{AB}\, r_{AB}\, \sin(\theta+\psi) + m_{BC}\, AB\, \sin\theta + m_{BC}\, r_{BC}\, \sin(\theta_{BC}+\psi_{BC}) + m_{CD}\, r_{CD}\, \sin(\theta_{CD}+\psi_{CD})\Big] \tag{3}$$

where m_{AB}, m_{BC} and m_{CD} are the masses of the blocks delimited by the respective hinges; r_{AB}, r_{BC}, r_{CD} are the distances between hinges A, B, D and the centres of mass G_1, G_2, G_3, respectively; AB denotes the length of the link delimited by hinges A and B; θ_{BC} and θ_{CD} are the rotation angles of the links BC and CD, functions of θ; ψ, ψ_{BC} and ψ_{CD} are the angles between links AB, BC, CD, respectively, and the centre of mass of the corresponding block. By deriving respect to θ Eq. (3) it results:

$$\frac{\partial V}{\partial\theta} = g m_{AB} r_{AB}\cos(\theta+\psi) + g\, m_{BC} AB\cos\theta + g m_{BC} r_{BC}\cos(\theta_{BC}+\psi_{BC})\frac{\partial\theta_{BC}}{\partial\theta} + g m_{CD} r_{CD}\cos(\theta_{CD}+\psi_{CD})\frac{\partial\theta_{CD}}{\partial\theta} \tag{4}$$

The critical rotation angle θ_{cr} can be evaluated by imposing a zero value of the first derivative of the potential energy expressed by Eq. (4).

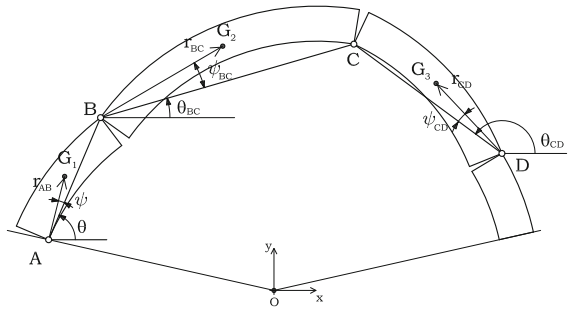

Fig. 5 Rotation angles and centres of mass related to mechanism Mech-l [6]

4.3 Equation of motion in the presence of geometrical uncertainties

Let us assume that mechanism Mech-l has been activated first, with hinges in position A, B, C, D (Fig. 3a). The equation of motion can be determined starting from Lagrange's equations:

$$\frac{\mathrm{d}}{\mathrm{d}t}\left(\frac{\partial T}{\partial\dot{\theta}}\right) - \frac{\partial T}{\partial\theta} + \frac{\partial V}{\partial\theta} = Q \tag{5}$$

where T is the kinetic energy of the system, V is the potential energy and Q the generalised forcing function related to the non-conservative forces. The equation of motion corresponding to a kinematics governed by mechanism Mech-l can be written in the following form

$$M_l(\theta)\,\ddot{\theta} + L_l(\theta)\,\dot{\theta}^2 + F_l(\theta)\,g = P_l(\theta)\,\ddot{x}_g \tag{6}$$

where the coefficients $M_l(\theta)$, $L_l(\theta)$, $F_l(\theta)$, $P_l(\theta)$, defined in [18], have been determined with reference to mechanism Mech-l, taking into account the geometrical irregularities when evaluating the inertial properties. The time history of the Lagrangian coordinate $\theta(t)$ completely describes the motion of the arch before an eventual impact occurs. Let us denote by θ_0 and $\dot{\theta}_0$ the initial conditions in terms of rotation and rota-

tional velocity at the beginning of the motion, namely at $t_0 = 0$. If the arch starts moving from its undisplaced configuration, corresponding to $\theta_0 = \theta_u$, equation of motion (6) is valid only for the condition $\theta < \theta_0$. The arch will move following mechanism Mech-l until an impact occur. In fact, after the first half cycle of motion, when it results again $\theta = \theta_0$, the arch returns to its start configuration: the joints corresponding to the four hinges A, B, C, D close and an impact occurs. At the instant of the impact, mechanism Mech-r will be activated, with hinges in position A', B', C', D' (Fig. 3b). Because of the geometrical uncertainties, after impact the hinges will not form in a symmetric configuration. Hence, when the kinematics is determined by mechanism Mech-r the equation of motion becomes:

$$M_r(\theta')\,\ddot{\theta}' + L_r(\theta')\,\dot{\theta}'^2 + F_r(\theta')\,g = -P_r(\theta')\,\ddot{x}_g \tag{7}$$

where the coefficients $M_r(\theta')$, $L_r(\theta')$, $F_r(\theta')$, $P_r(\theta')$ have been determined referring to mechanism Mech-r, considering the geometrical irregularities. Equation (7) must be solved with the initial conditions $\theta'_0 = \theta'_u$ and $\dot{\theta}'_0 = \dot{\theta}'_f$, being $\dot{\theta}'_f$ the rotational velocity of the equivalent link $A'B'$ immediately after impact. Hence, function $\theta'(t)$ that describes the motion after impact can be determined.

4.4 Impact modelling

The solution of the impact problem, consisting in the evaluation of the rotational velocity immediately after impact $\dot{\theta}'_f$, has been carried out according to the methodology proposed by De Lorenzis et al. [6].

Following Housner's approach related to the rocking block [16], impulsive forces associated with the impact are supposed to cause a variation of the rotational velocities and are applied at the opposite edges of the thickness respect to the collapse hinges. The value of the rotational velocity $\dot{\theta}'_f$ of the link $A'B'$ after impact is determined by imposing the equilibrium of linear and angular moments. Then, since the rotational velocity immediately before impact $\dot{\theta}_i$ is known, the coefficient of restitution can be defined:

$$c_v = \frac{\dot{\theta}'_f}{\dot{\theta}_i} \tag{8}$$

Following the observations provided by De Lorenzis et al. [6], once the geometrical parameters that define the shape of the nominal arch have been fixed (the angle of embrace α, the radius R of the mean circular construction line and the thickness t), the coefficient of restitution c_v can be evaluated. In this paper, as a first approximation, the value determined for the nominal geometry has been adopted also for the corresponding random arches.

5 Results

In the following, in order to investigate the influence of geometrical irregularities on the dynamic behaviour, results related to Oppenheim's arch NA are compared to those obtained from random arches RA-1 and RA-2. First, the trend of the potential energy is determined, by varying the value of the Lagrangian coordinate, to evaluate the critical rotational angle. Then, free vibrations problem and dynamic response under rectangular pulse base acceleration are analysed.

The geometries of the four-link mechanisms corresponding to Oppenheim's arch NA, arch RA-1 and arch RA-2 can be quickly defined. The undisplaced configuration at the instant of activation of mechanism Mech-l can be identified by the definition of the Lagrangian coordinate θ_u, the angles $\theta_{BC}(\theta_u)$ and $\theta_{CD}(\theta_u)$ and by the links length AB, BC and CD. With reference to Mech-r, the parameters θ'_u, $\theta'_{BC}(\theta'_u)$, $\theta'_{CD}(\theta'_u)$, $A'B'$, $B'C'$ and $C'D'$ identify the geometry of the four-link mechanism. The values of these parameters are reported in Table 2.

5.1 Effect of geometrical uncertainties on the critical rotation angle

Let us consider Oppenheim's arch NA and assume decreasing values of θ, starting from the undisplaced configuration corresponding to $\theta_0 = \theta_u$. At each value of the Lagrangian coordinate, the potential energy $V(\theta)$ is evaluated by means of Eq. (3). In Fig. 6, the trend of the potential energy for Oppenheim's arch is presented as a function of $\phi = \theta_u - \theta$ [18]. Starting from the undisplaced configuration, if θ decreases, the potential energy $V(\theta)$ increases until a maximum value is reached, corresponding to $\theta_{cr} = 0.8281$ ($\theta_u - \theta = 0.0691$). For values $\theta > \theta_{cr}$ the work done by the self-weight is negative, since it tends to bring the arch to the undisplaced configuration. For values $\theta < \theta_{cr}$ the trend

Table 2 Geometrical parameters of the four-link mechanisms corresponding to Oppenheim's arch NA, arch RA-1 and arch RA-2

	Oppenheim's arch NA	Arch RA-1	Arch RA-2	Unit measure
θ_u	0.8972	1.1454	1.1336	rad
$\theta_{BC}\,(\theta_u)$	− 0.3755	− 0.0828	− 0.1366	rad
$\theta_{CD}\,(\theta_u)$	2.3390	2.3569	2.3506	rad
AB	11.18	7.62	8.13	m
BC	7.78	10.99	10.85	m
CD	7.78	8.06	7.82	m
θ'_u	0.8972	1.1215	0.9002	rad
$\theta'_{BC}\,(\theta'_u)$	− 0.3755	− 0.1057	− 0.3504	rad
$\theta'_{CD}\,(\theta'_u)$	2.3390	2.3219	2.3263	rad
$A'B'$	11.18	7.86	11.10	m
$B'C'$	7.78	11.02	7.58	m
$C'D'$	7.78	7.72	8.06	m

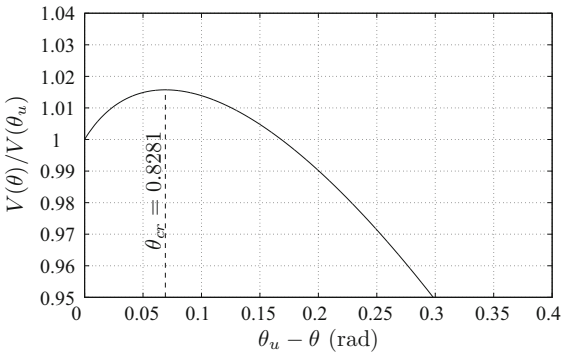

Fig. 6 Potential energy of Oppenheim's arch NA [18]

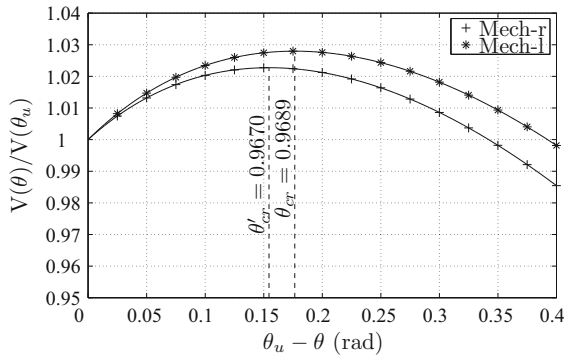

Fig. 7 Potential energy of arch RA-1 for Mech-l and Mech-r

of $V(\theta)$ decreases: the work done by the self-weight is positive because it tends to accommodate the displacements associated with the collapse mechanism [7].

The results related to Oppenheim's arch NA (Fig. 2) can be compared to those obtained by considering the uncertain geometries previously introduced (arch RA-1 and arch RA-2 depicted in Fig. 4). In Figs. 7 and 8, the trends of potential energy for the random arches are represented depending on $\phi = \theta_u - \theta$ ($\phi' = \theta'_u - \theta'$). Regarding arch RA-1, the values of the critical rotation angle are $\theta_{cr} = 0.9689$ ($\theta_u - \theta = 0.1765$) for Mech-l and $\theta'_{cr} = 0.9670$ ($\theta'_u - \theta' = 0.1545$) for Mech-r. For arch RA-2 it results $\theta_{cr} = 0.9613$ ($\theta_u - \theta = 0.1723$) and $\theta'_{cr} = 0.8375$ ($\theta'_u - \theta' = 0.0627$) for Mech-l and Mech-r, respectively. These results are summarised in Table 3 in terms of the ratio θ_{cr}/θ_u (or θ'_{cr}/θ'_u), which quantifies the displacement capacity of the arch, where the values θ_u (or θ'_u) correspond to the undisplaced configurations provided in Table 2. In particular, a high value of θ_{cr}/θ_u (or θ'_{cr}/θ'_u) indicates a small displacement capacity. From the results, it can be stated that the value of the potential energy has been modified by the geometrical uncertainties. The ratio θ_{cr}/θ_u (or θ'_{cr}/θ'_u) for random Oppenheim's arches may be lower or greater than that corresponding to Oppenheim's arch, namely the displacement capacity may be, respectively, bigger or smaller, depending on the geometrical uncertainties.

5.2 Free vibrations

The free vibrations of the arch have been studied following the analysis carried out by Clemente [5]. The

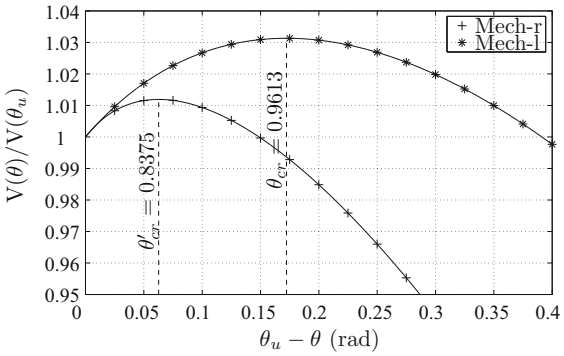

Fig. 8 Potential energy of arch RA-2 for Mech-l and Mech-r

Table 3 Ratio θ_{cr}/θ_u (or θ'_{cr}/θ'_u) between the critical rotation angle and the Lagrangian coordinate related to the undisplaced configuration

Arch geometry	θ_{cr}/θ_u (or θ'_{cr}/θ'_u)
Oppenheim's arch NA, Mech-n	0.923
Arch RA-1, Mech-l	0.846
Arch RA-1, Mech-r	0.862
Arch RA-2, Mech-l	0.848
Arch RA-2, Mech-r	0.930

arch at the instant $t_0 = 0$ has been released from an initial rotation of the mechanism Mech-l. The equation of motion (6) has been solved assuming zero ground acceleration and the following initial conditions in term of rotation and rotational velocity: $\theta_0 = \overline{\theta}$ and $\dot{\theta}_0 = 0$, with $\theta_u > \overline{\theta} > \theta_{cr}$. The initial conditions can be equivalently expressed in terms of the relative rotation $\phi = \theta_u - \theta$ between the undisplaced configuration and the displaced one: $\phi_0 = \overline{\phi}$ and $\dot{\phi}_0 = 0$.

A value of $\phi_0 = \theta_u - \theta_0 = 0.02$ has been assumed, so that $\theta_0 = \theta_u - \phi_0 > \theta_{cr}$ for all the analysed cases. First, the free vibrations have been studied with the assumption of a unitary value for the coefficient of restitution $c_v = 1$, namely assuming no energy dissipation during the impact. In Figs. 9, 10 and 11, the results for Oppenheim's arch NA, arch RA-1 and arch RA-2 are represented. As expected, the maximum amplitude of the oscillation for the random Oppenheim's arches is different, but constant, in each direction.

The free vibrations analysis has been repeated taking into account the dissipation of energy due to the impact. The coefficient of restitution c_v has been calculated for the Oppenheim's arch and found to be equal to $c_v = 0.875$. In Figs. 12, 13 and 14, the damped free vibrations for Oppenheim's arch NA, arch RA-1 and arch RA-2 are represented. As expected, the maximum amplitude of the oscillations in each direction decreases with time increase.

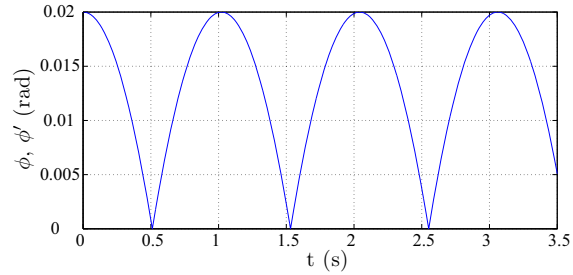

Fig. 9 Free vibrations of Oppenheim's arch NA for $c_v = 1$

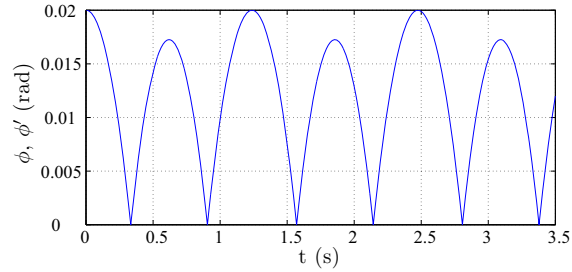

Fig. 10 Free vibrations of arch RA-1 for $c_v = 1$

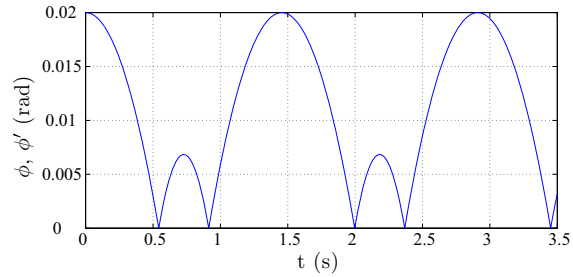

Fig. 11 Free vibrations of arch RA-2 for $c_v = 1$

5.3 Rectangular pulse base acceleration

5.3.1 Time history and initial conditions

The dynamic response to the idealised forcing function adopted by Oppenheim [18] has been analysed. The arches have been subjected to a pulse with constant ground acceleration $\ddot{x}_g$ and duration t_p, followed

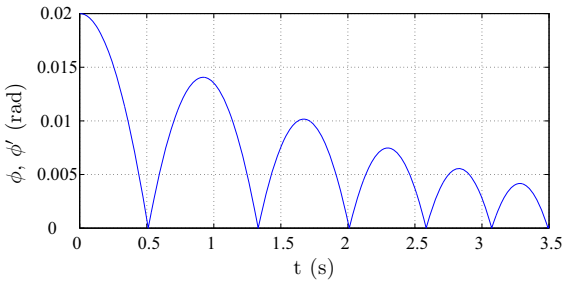

Fig. 12 Free vibrations of Oppenheim's arch NA for $c_v = 0.875$

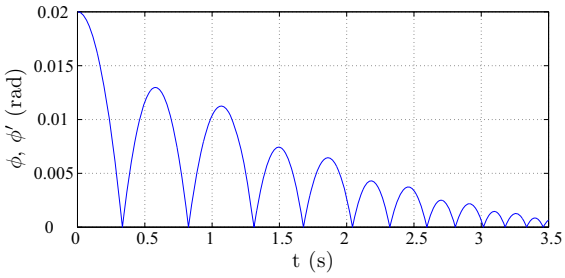

Fig. 13 Free vibrations of arch RA-1 for $c_v = 0.875$

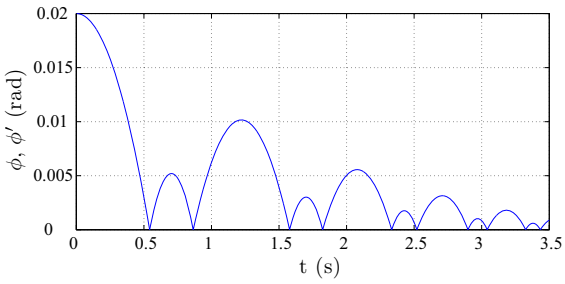

Fig. 14 Free vibrations of arch RA-2 for $c_v = 0.875$

by a pulse in the opposite direction having the half magnitude and twice the duration.

The arch motion has been determined depending on time, by solving alternatively Eqs. (6) and (7), considering the arch in its undisplaced configuration with zero initial velocity, subjected to the time history $\ddot{x}_g(t)$ from the instant $t_0 = 0$. The corresponding initial conditions related to mechanism Mech-l are $\theta_0 = \theta_u$ and $\dot{\theta}_0 = 0$, while for mechanism Mech-r it results $\theta'_0 = \theta'_u$ and $\dot{\theta}'_0 = 0$. The impact problem has been solved at each instant for which it results $\theta = \theta_u$ or $\theta' = \theta'_u$, depending on the type of mechanism involved (Mech-l or Mech-r), namely when the arch reaches the undisplaced configuration. The failure condition has been identified in correspondence of ever-increasing values of θ (or θ') or equivalently of ϕ (or ϕ'). It should be noted that for this type of impulse base acceleration, even if, as effect of the first pulse, the Lagrangian coordinate θ assumes values lower than the critical one θ_{cr} and the arch would tend to failure, it may or may not collapse depending on the magnitude and duration of the impulse in the opposite direction.

5.3.2 Effects of geometrical uncertainties on the dynamic response

In order to highlight the effects of geometrical uncertainties on the dynamic response, the results related to the Oppenheim's arch have been compared to those of the random arches. As an example, in the following, the arches have been subjected to the impulse base motions adopted by De Lorenzis et al. [6], corresponding to a value of the ground acceleration $\ddot{x}_g$ equal to $-1\,g$ with three different durations t_p equal to 0.44, 0.27 and 0.20 s. The results are shown in Fig. 15 for Oppenheim's arch NA, the random arches RA-1 and RA-2. The acceleration time histories are represented in Fig. 15a. The literature results by De Lorenzis et al. [6] regarding Oppenheim's arch have been found and they are presented by the blue curves of Fig. 15b–d, respectively, for t_p equal to 0.44, 0.27 and 0.20 s. Similarly, in the same figure, the dynamic responses of the random arches RA-1 and RA-2 are presented by red and green curves, respectively. The results related to the acceleration data $\ddot{x}_g = -1\,g$ and $t_p = 0.44$ s of Fig. 15b, show that Oppenheim's arch failure occurs during the first half cycle of motion without impacts, while the arches RA-1 and RA-2 collapse during the second half cycle of motion, after an impact has previously occurred. In Fig. 15c, the dynamic response for $\ddot{x}_g = -1\,g$ and $t_p = 0.27$ s is shown. The behaviour of the three arches is quite similar and characterized by the collapse during the second half cycle of motion after an impact, although the failure in the presence of geometrical uncertainties seems to occur for lower values of time respect to Oppenheim's arch NA. It is interesting the dynamic response to the impulse base acceleration of magnitude $\ddot{x}_g = -1\,g$ and duration $t_p = 0.20$ s, represented in Fig. 15d. It can be observed that both Oppenheim's arch NA and arch RA-1 recover after subsequent impacts, while arch RA-2 fails during the second half cycle of motion after an impact. In

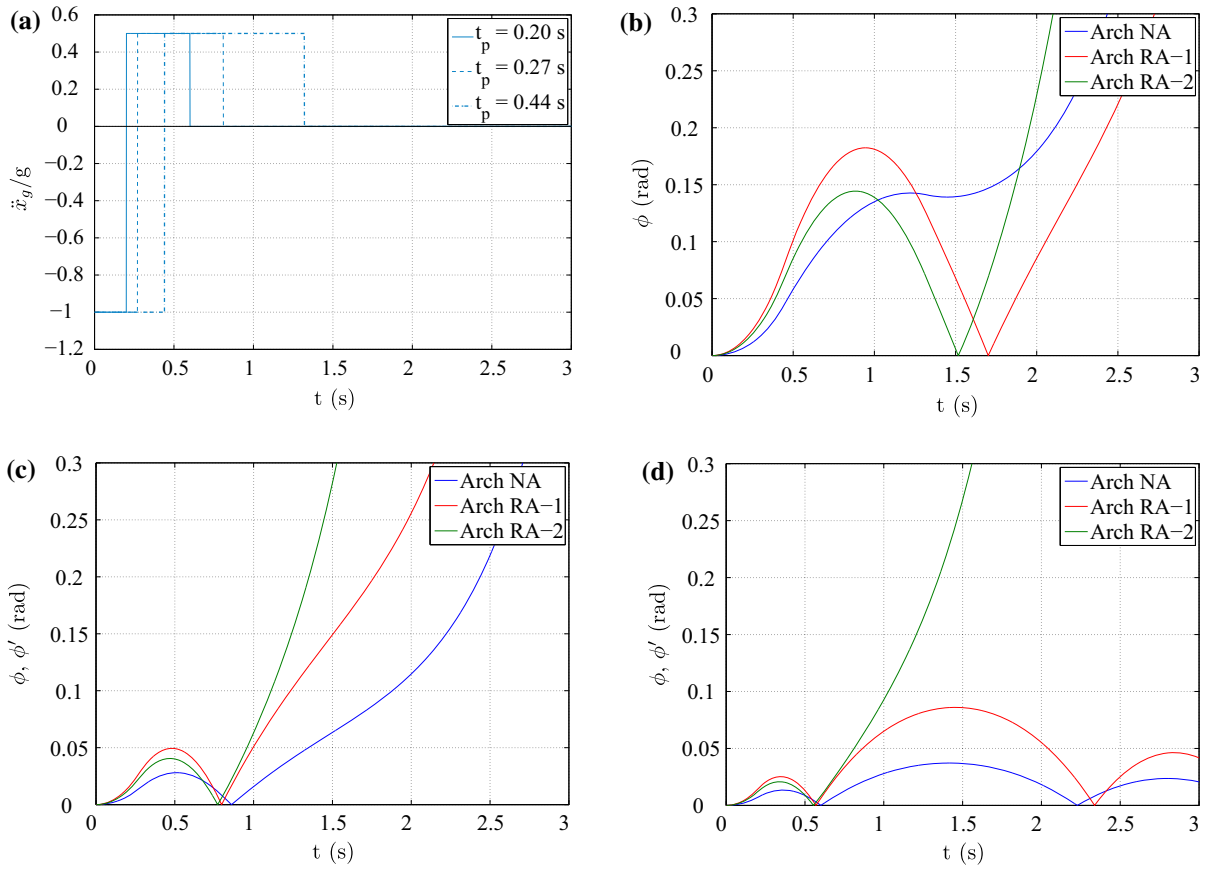

Fig. 15 Time history of the ground acceleration with $\ddot{x}_g = -1\,g$ (**a**) and dynamic response in terms of ϕ (or ϕ') for the Oppenheim's arch NA (blue), the arch RA-1 (red) and the arch RA-2 (green) for the cases $t_p = 0.44$ (**b**), $t_p = 0.27$ (**c**) and $t_p = 0.20$ (**d**)

this case, the uncertainties modified significantly the dynamic response.

5.3.3 Fragility curves

The dynamic analysis has been repeated by varying the magnitude of the acceleration $\ddot{x}_g$ and the duration t_p of the impulse base motion, in order to determine the failure domains provided by Oppenheim [18] and De Lorenzis et al. [6]. The results, which refer to a nominal geometry, are represented in Fig. 16. The continuous black line with asterisks corresponds to the boundary related to the failure during the first half cycle of motion and is the same as that obtained by Oppenheim [18]. The boundary corresponding to failure during the second half cycle of motion is represented by the black continuous dotted curve, which is coincident with the curve by De Lorenzis et al. [6]. This curve gives the collapse condition of the arch in terms of peak acceleration and time duration and it will be called the *failure curve*. The horizontal black dashed line in Fig. 16 indicates the horizontal load multiplier of Oppenheim's arch $k = 0.37$, determined by limit analysis, below which there is no activation of the motion for this deterministic arch, which moves rigidly with the ground. This limit may not be valid for arches with geometrical uncertainties, as observed in Sect. 3. For more details on the calculation of the horizontal load multiplier by limit analysis, following a probabilistic approach, see [4]. Region (1) in Fig. 16, between the horizontal dashed black line and the failure curve, corresponds to states of recovery for Oppenheim's arch; region (2) identifies the states of collapse during the second half cycle of motion, while region (3) above the upper curve with asterisk corresponds to failure conditions during the first half cycle of motion [6].

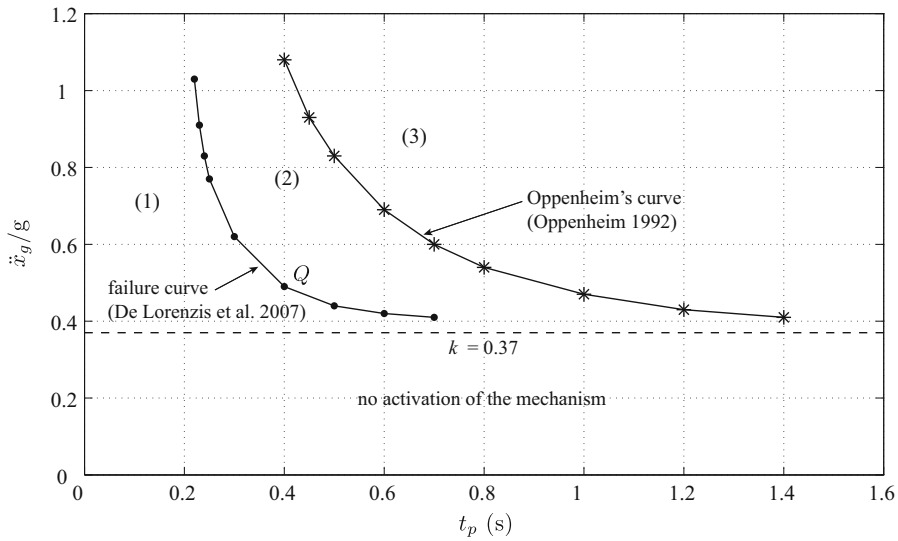

Fig. 16 Failure domain for Oppenheim's arch ($\varepsilon = 0$) related to an impulse base motion with duration t_p and magnitude acceleration $\ddot{x}_g$: region of recovery (1), collapse after the second half cycle of motion (2) and collapse after the first half cycle of motion (3) [6,8,18]

In order to quantify the effect of the geometrical uncertainties on the collapse condition in the dynamic field, *fragility curves* were obtained. Each fragility curve corresponds to a fixed value of impulse duration and was determined according to the procedure described below. A sample of $h = 40$ random Oppenheim's arches were generated, following the methodology described at Sect. 2. Values of the impulse duration $\bar{t}_p$ equal to 0.4, 0.5, 0.6, 0.7 s were considered. At each one of these, increasing values of the acceleration magnitude $\ddot{x}_g$ were applied, with an interval equal to $0.01\,g$. For each couple $(\bar{t}_p,\ \ddot{x}_g)$, dynamic analysis was performed on the h elements of the generated sample of random arches; the dynamic analysis was executed twice for each arch, since both directions of ground motion were considered. Then, the estimated cumulative probability of failure P_F was calculated as follows:

$$P_F(\bar{t}_p,\ \ddot{x}_g) = \frac{h_f(\bar{t}_p,\ \ddot{x}_g)}{h} \tag{9}$$

where $h_f(\bar{t}_p,\ \ddot{x}_g)$ is the number of random arches that failed in the presence of an impulse base motion having time duration $\bar{t}_p$ and magnitude acceleration $\ddot{x}_g$, with $h_f \leq h$. The fragility curve at a fixed value of the impulse duration $\bar{t}_p$ can be obtained by presenting the estimated cumulative probability of failure P_F depending on the acceleration magnitude $\ddot{x}_g$. In particular, the fragility curve for Oppenheim's arch, when the geometrical uncertainties are neglected, can be defined as follows:

$$\begin{cases} P_F(\bar{t}_p,\ \ddot{x}_g) = 0 & \text{if } \ddot{x}_g < \overline{\ddot{x}}_g \\ P_F(\bar{t}_p,\ \ddot{x}_g) = 1 & \text{if } \ddot{x}_g \geq \overline{\ddot{x}}_g \end{cases} \tag{10}$$

where $\bar{t}_p$ and $\overline{\ddot{x}}_g/g$ are the coordinates of the point Q belonging to the failure curve of Fig. 16.

In Fig. 17, the fragility curve for the random Oppenheim's arch (in the presence of geometrical uncertainties), related to the case $\bar{t}_p = 0.40$ s, is presented by the dashed black line that approximates (fifth degree polynomial function) the numerical results (black dots). The vertical dash-dot black line corresponds to the failure acceleration $\overline{\ddot{x}}_g = 0.49\,g$ of the Oppenheim's arch (without geometrical uncertainties). In the same figure, the results obtained by means of limit analysis, when the dynamic behaviour is not considered, have been represented by a blue colour. Following the procedure proposed by Cavalagli et al. [4], a set of $s = 1000$ random Oppenheim's arches has been generated using the uniform probability density functions of Fig. 1c. For each random arch, two values of the horizontal load multiplier have been determined by limit analysis, denoted as $\tilde{k}_l$ and $\tilde{k}_r$. Then, the minimum value between them has been determined $\tilde{k} = \min(\tilde{k}_l,\ \tilde{k}_r)$. The blue continuous curve of Fig. 17 represents the estimation of the cumulative probability function of the horizontal load multiplier $\tilde{k}$. This curve provides an interesting comparison with the dashed black curve, since it

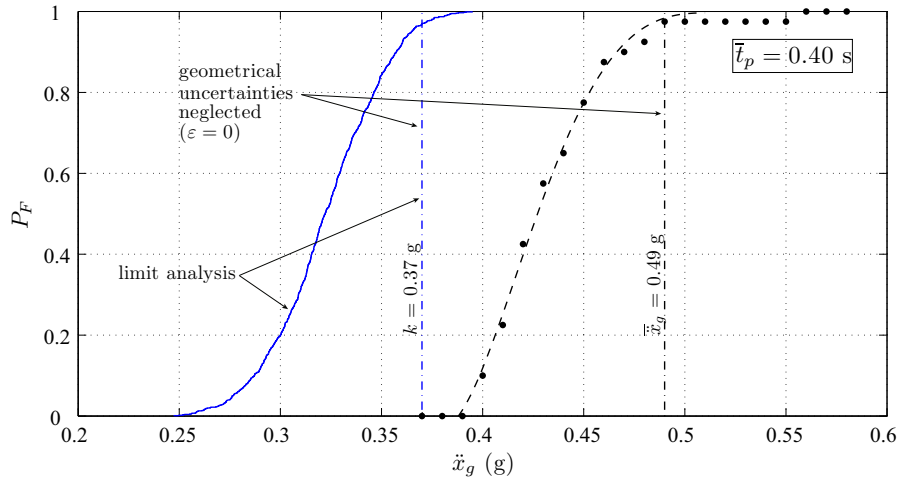

Fig. 17 Fragility curve for random Oppenheim's arch ($\varepsilon = 0.10$) corresponding to $t_p = 0.40$ s (black dashed curve with dots) and estimation of the cumulative probability function of the random horizontal load multiplier $\bar{k}$ determined by limit analysis (blue continuous curve). The vertical lines represent the accelerations of activation of the mechanism when the geometrical uncertainties are not taken into account ($\varepsilon = 0$): limit analysis (blue line) or dynamic analysis under rectangular pulse base acceleration (black line). (Color figure online)

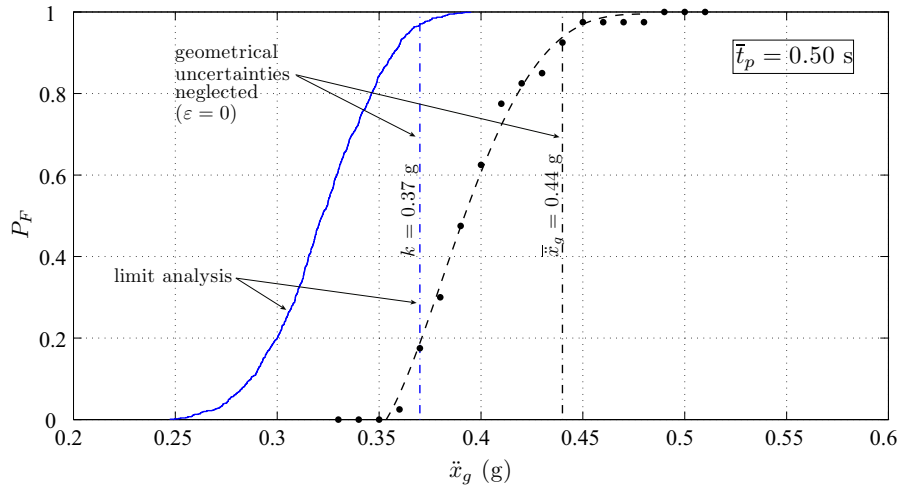

Fig. 18 Fragility curve for random Oppenheim's arch ($\varepsilon = 0.10$) corresponding to $t_p = 0.50$ s (black dashed curve with dots) and estimation of the cumulative probability function of the random horizontal load multiplier $\bar{k}$ determined by limit analysis (blue continuous curve). The vertical lines represent the accelerations of activation of the mechanism when the geometrical uncertainties are not taken into account ($\varepsilon = 0$): limit analysis (blue line) or dynamic analysis under rectangular pulse base acceleration (black line). (Color figure online)

identifies the probability of collapse in the presence of geometrical uncertainties when the dynamic effects are not considered. The vertical dash-dot blue line corresponds to the horizontal load multiplier k determined for Oppenheim's arch without geometrical uncertainties, by means of limit analysis.

Similarly, in Figs. 18, 19 and 20 the fragility curves related, respectively, to the cases $\bar{t}_p = 0.50,\ 0.60,\ 0.70$ s have been represented (black dashed curves with dots), together with the cumulative probability function of the horizontal load multiplier determined by limit analysis (blue continuous curves).

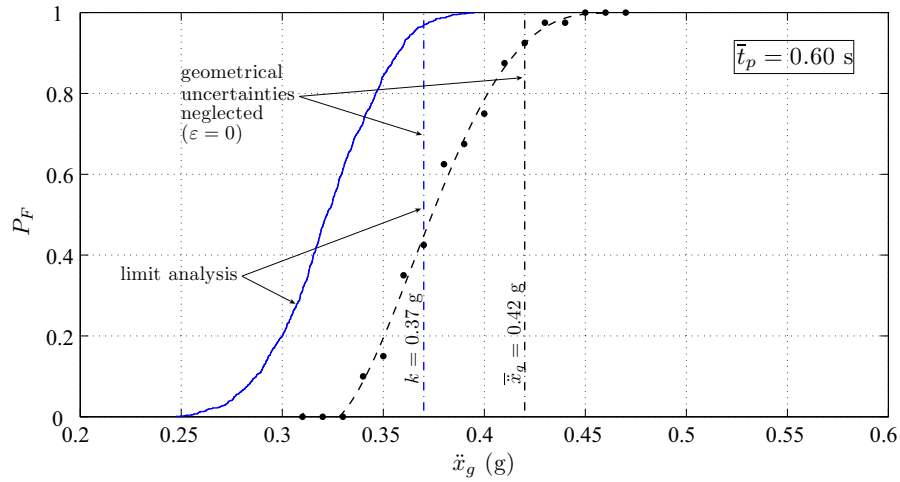

Fig. 19 Fragility curve for random Oppenheim's arch ($\varepsilon = 0.10$) corresponding to $t_p = 0.60$ s (black dashed curve with dots) and estimation of the cumulative probability function of the random horizontal load multiplier $\tilde{k}$ determined by limit analysis (blue continuous curve). The vertical lines represent the accelerations of activation of the mechanism when the geometrical uncertainties are not taken into account ($\varepsilon = 0$): limit analysis (blue line) or dynamic analysis under rectangular pulse base acceleration (black line). (Color figure online)

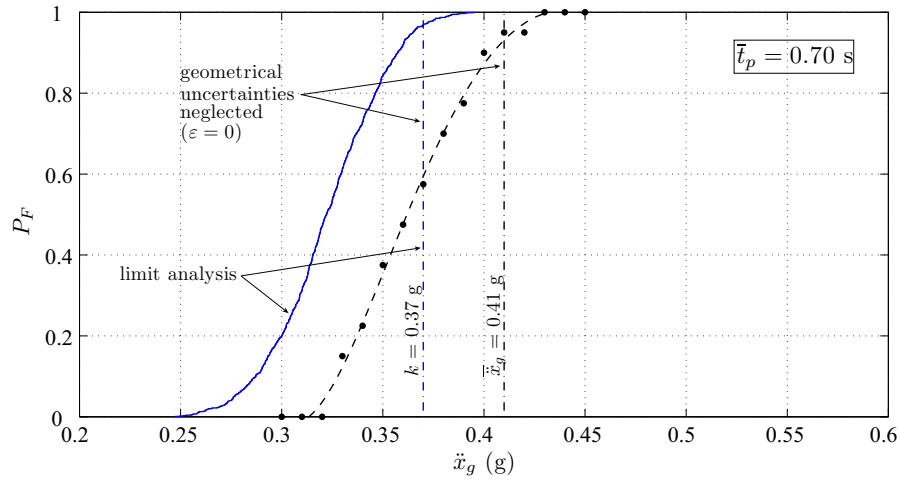

Fig. 20 Fragility curve for random Oppenheim's arch ($\varepsilon = 0.10$) corresponding to $t_p = 0.70$ s (black dashed curve with dots) and estimation of the cumulative probability function of the random horizontal load multiplier $\tilde{k}$ determined by limit analysis (blue continuous curve). The vertical lines represent the accelerations of activation of the mechanism when the geometrical uncertainties are not taken into account ($\varepsilon = 0$): limit analysis (blue line) or dynamic analysis under rectangular pulse base acceleration (black line). (Color figure online)

An effective representation of the sensitivity of failure conditions with respect to geometrical uncertainties is given by the *fragility surface* of the random Oppenheim's arch shown in Fig. 21 (corresponding to a value of the tolerance equal to $\varepsilon = 0.10$). This surface has been obtained connecting, by means of plane surfaces, the fragility curves of Figs. 17, 18, 19 and 20. The vertical curved surface corresponds to the failure surface for Oppenheim's arch when the geometrical uncertainties are neglected. The fragility surface for Oppenheim's

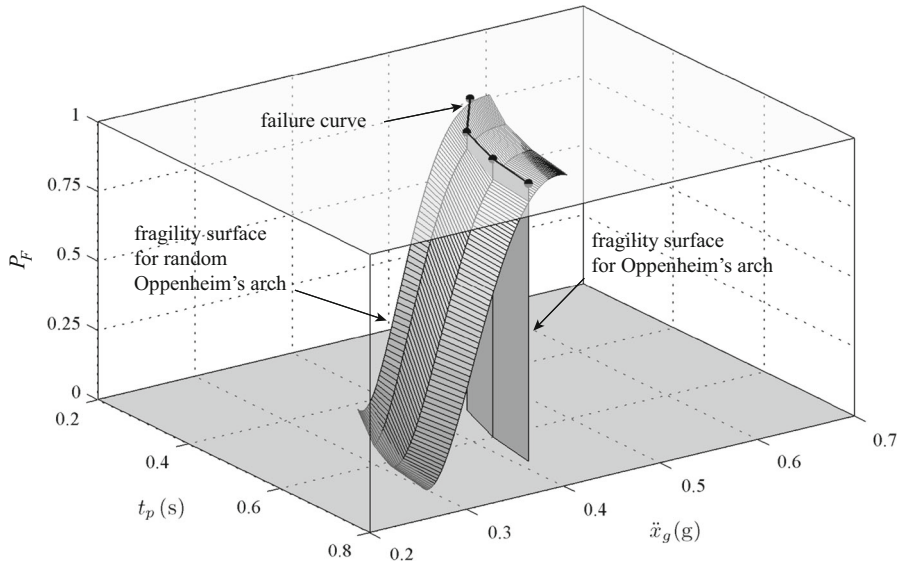

Fig. 21 Fragility surface for random Oppenheim's arch ($\varepsilon = 0.10$), superimposed to the cylindric vertical surface representing the fragility surface for Oppenheim's arch ($\varepsilon = 0$)

arch generally overestimates the dynamic resistance if geometrical uncertainties are considered. In fact, a portion of the fragility surface for the random Oppenheim's arch lies on the side of lower values of magnitude acceleration, compared to the cylindrical fragility surface. In other words, if the geometrical uncertainties are neglected, an estimated cumulative probability of failure $P_F = 0$ is predicted, while actually it may be different respect to zero.

6 Conclusions

From the understanding that the stability of the masonry arch, while adopting Heyman's hypotheses, is essentially a geometrical equilibrium problem (between the arch geometry and the thrust line, which in turn depends on the geometry), it follows that geometrical irregularities can play therefore a crucial role. In this paper, to verify this conjecture, the dynamic behaviour of the masonry arch has been investigated taking into account geometrical uncertainties that could be related to defects of shape of the voussoirs, imprecision of construction or deterioration due to environmental factors. The non linear dynamical model of Oppenheim's arch has been adopted, where the dissipation of energy, due to impact between the rigid blocks, has been modelled following the approach proposed by De Lorenzis et al., estimating the resulting reduction of the rotational velocity. Assuming Oppenheim's arch as deterministic or nominal arch, the geometrical uncertainties have been included in the dynamic analysis considering arches with random geometry; in particular, the radius of the mean circular construction line of the arch, the thickness and the angle of embrace of each voussoir have been assumed as random variables, with independent uniform probability density functions. The dynamic behaviour of the generated samples has been investigated under a step impulse base acceleration. The results confirmed that geometrical uncertainties modify the dynamic behaviour of the arch, and that even if a deterministic calculation predicts recovery after subsequent impacts, failure may occur when geometrical uncertainties are considered. Moreover, the fragility surface of the arch versus the characteristics of step impulse base acceleration (duration and peak acceleration) has been estimated; this surface identifies the three-dimensional failure domain of the arch with geometrical uncertainties. More analyses are necessary in order to consider different types of acceleration time histories, such as harmonic or earthquake excitation. It could also be interesting to investigate the effects of uncertainties on different nominal geometries or arch shapes. However, obtained results highlight that geometrical irregularities should be considered while studying the dynamic stability of the masonry arch and this should be especially taken into account when conducting a seismic vulnerability analysis.

Acknowledgements The research has been partially supported by the project "Advanced mechanical modelling of new materials and structures for the solution of 2020 Horizon challenges"

funded by the Italian Ministry of Education, University and Scientific Research, within the PRIN National Grant 2015 (Prot. 2015JW9NJT).

Compliance with Ethical Standards

Conflict of Interest: The authors declare that they have no conflict of interest.

References

1. De Arteaga, I., Morer, P.: The effect of geometry on the structural capacity of masonry arch bridges. Constr. Build. Mater. **34**, 97–106 (2012)
2. Caporale, A., Feo, L., Hui, D., Luciano, R.: Debonding of FRP in multi-span masonry arch structures via limit analysis. Compos. Struct. **108**, 586–865 (2014)
3. Cavalagli, N., Gusella, V., Severini, L.: Lateral loads carrying capacity and minimum thickness of circular and pointed masonry arches. Int. J. Mech. Sci. **115–116**, 645–656 (2016)
4. Cavalagli, N., Gusella, V., Severini, L.: The safety of masonry arches with uncertain geometry. Comput. Struct. **188**, 17–31 (2017)
5. Clemente, P.: Introduction to dynamics of stone arches. Earthq. Eng. Struct. Dyn. **27**, 513–522 (1998)
6. De Lorenzis, L., DeJong, M., Ochsendorf, J.: Failure of masonry arches under impulse base motion. Earthq. Eng. Struct. Dyn. **36**, 2119–2136 (2007)
7. De Santis, S., de Felice, G.: A fibre beam-based approach for the evaluation of the seismic capacity of masonry arches. Earthq. Eng. Struct. Dyn. **43**, 1661–1681 (2014)
8. DeJong, M.: Seismic assessment strategies for masonry structures. PhD dissertation, Massachusetts Institute of Technology (2009)
9. DeJong, M., De Lorenzis, L., Adams, S., Ochsendorf, J.: Rocking stability of masonry arches in seismic regions. Earthq. Spectra **24**, 847–865 (2008)
10. DeJong, M., Dimitrakopoulos, E.: Dynamically equivalent rocking structures. Earthq. Eng. Struct. Dyn. **43**, 1543–1563 (2014)
11. DeJong, M., Ochsendorf, J.: Analysis of vaulted masonry structures subjected to horizontal ground motion. In: Lourenço, P.B., Roca, P., Modena, C., Agrawal, S. (eds.) Proceedings of the 5th international conference on structural analysis of historical constructions, vol. 2, pp. 973–980 (2006)
12. Dimitri, R., De Lorenzis, L., Zavarise, G.: Numerical study on the dynamic behavior of masonry columns and arches on buttresses with the discrete element method. Eng. Struct. **33**, 3172–3188 (2011)
13. Dimitri, R., Tornabene, F.: A parametric investigation of the seismic capacity for masonry arches and portals of different shapes. Eng. Fail. Anal. **52**, 1–34 (2015)
14. Heyman, J.: The safety of masonry arches. Int. J. Mech. Sci. **11**, 363–385 (1969)
15. Heyman, J.: The Masonry Arch. Ellis Horwood Ltd., Chinchester (1982)
16. Housner, G.: The behavior of inverted pendulum structures during earthquakes. Bull. Seismol. Soc. Am. **53**(2), 403–417 (1963)
17. Misseri, G., Rovero, L.: Parametric investigation on the dynamic behaviour of masonry pointed arches. Arch. Appl. Mech. **87**, 385–404 (2017)
18. Oppenheim, I.: The masonry arch as a four-link mechanism under base motion. Earthq. Eng. Struct. Dyn. **21**, 1005–1017 (1992)
19. Psycharis, I.N., Papastamatiou, D., Alexandris, A.: Parametric investigation of the stability of classical columns under harmonic and earthquake excitations. Earthq. Eng. Struct. Dyn. **29**, 1093–1109 (2000)
20. Riveiro, B., Solla, M., De Arteaga, I., Arias, P., Morer, P.: A novel approach to evaluate masonry arch stability on the basis of limit analysis theory and non-destructive geometric characterization. Autom. Constr. **31**, 140–148 (2013)
21. Zampieri, P., Zanini, M., Faleschini, F.: Influence of damage on the seismic failure analysis of masonry arches. Constr. Build. Mater. **119**, 343–355 (2016)
22. Zanaz, A., Yotte, S., Fouchal, F., Chateauneuf, A.: Efficient masonry vault inspection by monte carlo simulations: case of hidden defect. Case Stud. Struct. Eng. **5**, 1–12 (2016)